A Dual-Mode Monoblock Dielectric Bandpass Filter Using Dissimilar Fundamental Modes

Yuliang Chen, *Graduate Student Member, IEEE*, Yan Zhang, and Ke-Li Wu, *Fellow, IEEE*

***Abstract*— In this article, a novel dual-mode monoblock dielectric resonator (MDR) for compact monoblock dielectric bandpass filters is presented and put into practical use for the first time. In the dual-mode resonator, two dissimilar TEM modes are generated by forming two perpendicular metalized blind holes in a silver-coated cuboid-shapes dielectric block. The resonator can maximize the space utilization with up to 50% volume reduction while maintaining a wide spurious-free frequency band. The coupling of the two modes in such a resonator can be effectively controlled by one or more partial-height metalized posts. A convenient input/output (I/O) coupling scheme for surface-mount applications is introduced, and versatile coupling arrangements for realizing various filter characteristics are presented. To demonstrate the proposed filter miniaturization technique, a six-pole inline bandpass filter with one pure imaginary transmission zero (TZ) in a 3.5-GHz band is electromagnetic (EM) designed, and a ten-pole symmetric bandpass filter with two pure imaginary TZs in a 2.6-GHz band of fifth-generation (5G) new radio (NR) frequency band is designed, prototyped, and tuned. Experimental results show that the proposed dual-mode MDR filter can obtain an acceptable RF performance for 5G applications with a significant volume reduction compared to existing single-mode solutions.**

***Index Terms*— Dual-mode resonator, filter miniaturization technique, monoblock dielectric resonator (MDR) filter.**

I. Introduction

DIELECTRIC resonator (DR) filters have been widely used in terrestrial and space communication systems due to their relatively compact size, higher unloaded Q-factor, and better thermal stability compared to conventional metallic cavity filters. Since practical implementations of DR filters were attempted by Harrison and Cohn in the 1960s [1], [2], tremendous research efforts have been devoted to the design methodologies and viable realization options of DR microwave filters, including electromagnetic (EM) modeling, exploration of different resonant modes, and various miniaturization techniques. The early works on DR filters were well-reviewed in [3]. Presently, the available DR microwave filter configurations can be classified into two categories: DR-loaded metal cavity filters and monoblock DR (MDR) filters. The resonant mode and the unloaded Q of the former are determined by the shape and electrical size of the loaded DR and the association of the DR with the metal housing, whereas those of the latter are only determined by the size and the geometry of the dielectric block as the metallic housing is formed by the conductive metal plated on the outer surface of the dielectric block.

For a given dielectric constant of a DR, without significantly sacrificing unloaded Q, the most effective way to reduce the overall size of a filter is to realize multiple electric resonators in the same physical resonator, namely, the multiple-mode resonator. This concept is first adopted in metallic cavity filters and then naturally used in DR-loaded metal cavity filters. The earliest dual-mode DR filter was reported in [4], in which a pair of degenerate modes whose field patterns show strong resemblance with those of TE_{111} modes in a circular waveguide cavity are supported by mounting the DR axially in a cylindrical metal cavity. To realize a more compact dual-mode DR-loaded resonator, the dual TM_{110} (also called HE_{11}) modes are considered to be the most popular degenerate modes in various applications [5]–[8]. With an appropriate dimension tradeoff and a tactical geometry modification, the degenerate TM_{110} modes can be managed to be the fundamental mode. Of course, exploration of higher degrees of degenerate modes in the same physical metal cavity has never been stopped. Such resonator configurations include the triple-mode DR-loaded resonators [9] and the quadruple-mode DR-loaded resonators [10], [11]. Usually, the higher the degree of degeneracy, the poor the independent controlling. The intrinsic issues of a degenerate multimode DR-loaded resonator are obvious, which includes: 1) the mode spectrum depends on the size and shape of the metal housing; 2) the size of a DR-loaded resonator that supports degenerate modes is usually larger than that of the fundamental mode DR-loaded resonator, resulting in limited space-saving; and 3) poor spurious mode performance compared to a single fundamental mode resonator. A new type of mixed-mode resonator consisting of a waveguide cavity and a loaded DR is proposed in [12], in which uncoupled cavity TE_{101} and dielectric $TE_{10\delta}$ modes are employed within the same volume.

The MDR filter, on the other hand, is more straightforward in structure and more compact in size. MDR filters can be formed in a combline structure with TEM mode resonators [13]–[15], the waveguide structure with non-TEM mode resonators [16]–[19], and the dielectric rod loaded resonator structure with TM_{01} mode [20]. With the wide

Manuscript received November 28, 2020; revised March 9, 2021; accepted May 10, 2021. Date of publication June 28, 2021; date of current version August 5, 2021. This work was supported by the Postgraduate Scholarship from The Chinese University of Hong Kong. *(Corresponding author: Ke-Li Wu.)*

The authors are with the Department of Electronic Engineering, The Chinese University of Hong Kong, Hong Kong (e-mail: ylchen@link.cuhk.edu.hk; yzhang@link.cuhk.edu.hk; klwu@cuhk.edu.hk).

Color versions of one or more figures in this article are available at https://doi.org/10.1109/TMTT.2021.3089720.

Digital Object Identifier 10.1109/TMTT.2021.3089720

adoption of massive multi-input–multi-output (M-MIMO) antenna arrays in the fifth-generation (5G) wireless communication systems, the specifications for the filters that are immediately cascaded to each of the antenna elements have become ever-stringent with the primary constrain on the size of the filters. Subject to the cost-effectiveness in mass production, MDR filters have been receiving tremendous attention from the industry. To further reduce the size of a waveguide MDR, the concept of ridge-loaded waveguide resonator was first used in low temperature co-fired ceramics (LTCC) chip filters [21] and then was employed to support a quasi-TEM mode in an MDR filter [22]. In designing an MDR filter, one of the challenges is how to create transmission zeros (TZs) flexibly, for which an effective way to realize negative coupling is essential. An innovative way to realize negative coupling in an MDR filter is to use a partial-height conductive post [23], which was originally proposed as a dispersive coupling element [24], [25]. Single- and double-folded structures can also be used for realizing certain compact MDR filter configurations [26], [27]. An attempt is made to utilize a triple degenerate waveguide mode MDR filter [28]. Although a high-Q attribute is achieved and a wide spurious-free frequency band is observed by cascading a single-mode resonator on each side of the triple-mode resonator cube, the filter structure is bulky and is difficult to mass-produce. Since multiple segregated DR blocks need to be assembled and bonded together delicately, strictly speaking, the filters reported in [26]–[28] are not monoblock configurations. To the best of our knowledge, there is no truly MDR filter that employs multiple-mode resonators in the literature. Despite that MDR filters have shown their vitality in various wireless applications, including the 5G systems, the research on their volume reduction while retaining design flexibility and manufacturability would be highly desired.

Recently, an innovative idea to create a dual-mode resonator using two dissimilar modes in one physical waveguide cavity was reported [29]. With the dual-mode resonator, the input/output (I/O) feeding probe is tapped to a horizontally situated three-quarter wavelength long coaxial resonator, which is, in turn, coupled to the TE_{101} mode in the terminal rectangular waveguide resonator. A further study in [30] suggests that an auxiliary cylindrical post can be introduced to increase the coupling between the two dissimilar modes. Due to limited flexibility in waveguide resonators, the dual-mode resonator only serves as the I/O resonator, while other resonators of the filter are still conventional single-mode waveguide resonators.

Inspired by the work in [29] and [30], a new type of dual-mode MDR is proposed in this article. The resonator supports two dissimilar fundamental modes: one is the quasi-TEM mode supported by a partial-height metal post loaded dielectric waveguide cavity and the other is the TEM mode provided by a quarter-wavelength long metal post (coaxial resonator) that is horizontally projected from a sidewall of the cavity. To effectively reduce the coupling of the two tightly coupled dissimilar modes, a metalized blind hole extending from the opposite side of the partial-height metal post for supporting the quasi-TEM mode is introduced. Besides, various coupling topologies utilizing the proposed dual-mode resonator for

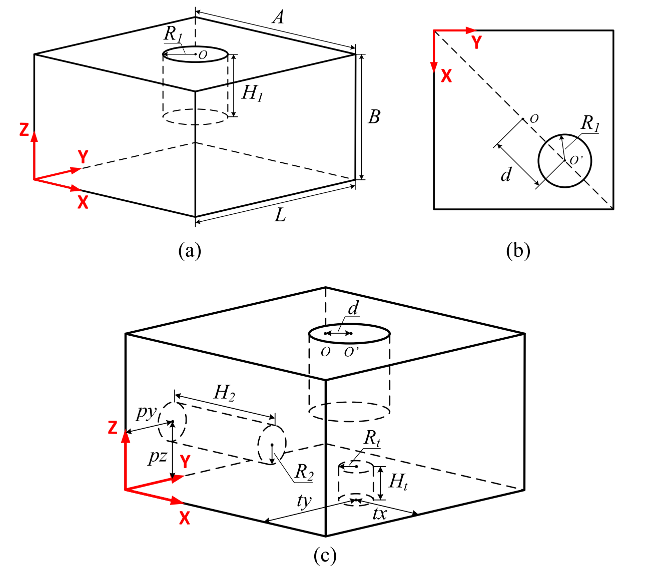

Fig. 1. (a) Isometric view of the quasi-TEM mode resonator. (b) Top view of the resonator in (a) with offset distance d from the center of the top surface. (c) Isometric view of the proposed dual-mode resonator with a decoupling post.

constructing compact MDR filters are discussed, demonstrating high flexibility in designing high-performance bandpass filters. Comparing to existing MDR filters, the proposed dual-mode MDR filter possesses the following unique and attractive features: 1) it virtually offers the space-saving ratio up to 2, which is the highest achievable volume reduction ratio for dual-mode filters; 2) it is a truly monolithic structure that is suitable for mass production without assembling and bonding process; 3) it allows a high degree of flexibility in coupling layout for achieving TZs; and 4) it exhibits a wide spurious-free frequency band.

In this article, the concept of the dual-mode MDR filter will be demonstrated by two design examples: an EM designed six-pole MDR bandpass filter working in the 3.5-GHz band of 5G systems with one TZ in the high rejection band and a fabricated ten-pole MDR bandpass filter operating in the 2.6-GHz band of 5G systems with one TZ on each side of the passband. The ten-pole prototyped filter consists of four proposed dual-mode resonators and two single-mode resonators. The experimental result of the prototyped filter justifies the usefulness of the proposed dual-mode resonator and shows that the proposed resonator configuration can significantly reduce the volume of the existing single-mode counterpart with good RF performance. The design examples further demonstrate that the dual-mode resonator is a viable candidate for the applications of M-MIMO radio units in 5G and future wireless communication systems.

II. Dual-Mode MDR

The basic structure of the proposed dual-mode MDR is presented in Fig. 1. In the EM parametric analysis, it is assumed that the resonant frequency f_0 is set to 2.6 GHz, and the dielectric material is with relative permittivity $\varepsilon_r = 20.6$, the loss tangent $\tan\delta = 5 \times 10^{-5}$, and the metal conductivity of the silver coating layer $\sigma = 3.5 \times 10^7$ S/m. The loss model for EM simulation is pertinent to the prototype production process and has been verified by a number of experimental prototypes. To provide a realistic and practical picture through the parametric study, the size of the single resonator is set to $10.5 \times 10.5 \times 6$ mm^3 in all examples of this section.

A. Dual-Mode MDR

With the given dimensions of the cuboid resonator block, the resonant frequency for the fundamental TE_{101} mode is at 4.45 GHz, which is much higher than the target frequency of 2.6 GHz. To lower the resonant frequency, a cylindrical post formed by a metalized blind hole is inserted along the vertical direction from the top surface of the dielectric block. As shown in Fig. 1(a), the cavity with width $A = 10.5$ mm, length $L = 10.5$ mm, and height $B = 6$ mm together with the vertical cylindrical post with radius R_1 and depth H_1 located near the center of the top surface forms a quasi-TEM mode (mode 1) resonator. The offset distance d of the center of the post from the center of the cavity in a diagonal direction, as defined in Fig. 1(b), can be adjusted to control the coupling of the dual modes. This kind of ridge-loaded DR has been well known in the industry.

The second mode (mode 2) in the resonator is formed by inserting a metalized quarter-wavelength long post horizontally into the resonator cavity of mode 1. The post is short-circuited with a metalized side wall at one end and open-circuited at the other. The second resonator supports a TEM mode. Again, the post can be formed by a metalized blind hole. As shown in Fig. 1(c), the center of the short-circuited end of the post, which is with radius R_2 and length H_2, is positioned at (*0*, *py*, *pz*) in the *YOZ* plane. The second resonator can also be formed by a three-quarter wavelength long one-end-short and one-end-open resonator post or a half-wavelength long TEM mode resonator with both ends open-circuited. In this article, only the quarter-wavelength long TEM mode resonator is considered.

With a fixed radius $R_1 = 1.5$ mm, the resonant frequency of the quasi-TEM mode (mode 1) f_1 can be adjusted by varying the depth H_1. By a simple parametric study with two typical values of the offset distance d, the resonant frequency f_1 and the corresponding unloaded Q-factor are plotted in Fig. 2(a). It can be seen that, for $d = 0$ mm and $H_1 = 3.8$ mm, $f_1 = 2.6$ GHz with $Q = 1223$. When the post is offset from the center of the top surface, the Q-factor of the quasi-TEM mode resonator will deteriorate. Therefore, to obtain a higher Q resonator, the post should be placed as close to the center as possible.

To investigate the resonant frequency and unloaded Q of the second mode, i.e., the TEM mode resonator, the resonator dimensions are chosen as $R_1 = 1.5$ mm, $H_1 = 3.8$ mm, and $d = 0$ mm, whereas the quasi-TEM mode resonator is detuned by short-circuiting the vertical post. The parametric study by varying length H_2 with a different radius R_2 is presented in Fig. 2(b), for which $py = 2.5$ mm and $pz = 2.3$ mm. It can be observed that, when $R_2 = 0.75$ mm, the actual length H_2 for $f_0 = 2.6$ GHz is 4.8 mm, which is shorter than the theoretical

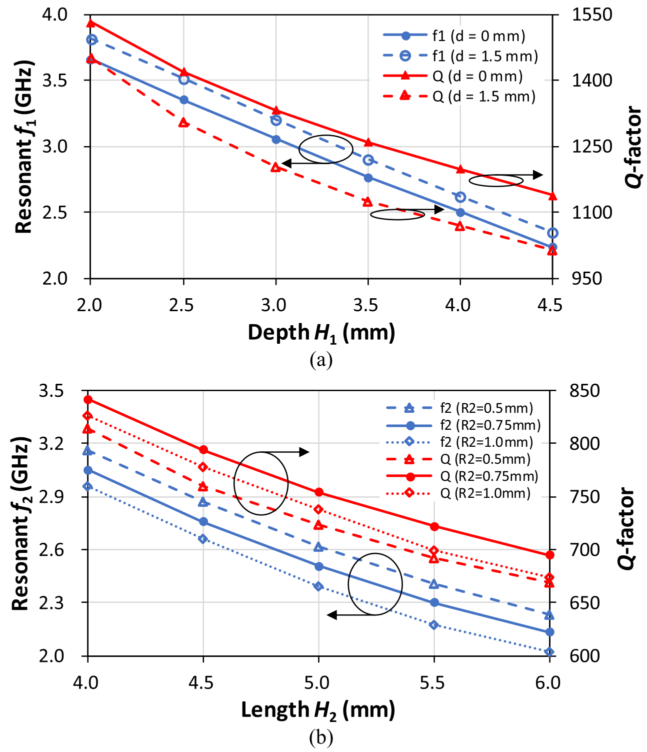

Fig. 2. (a) Resonant frequency of the quasi-TEM mode (f_1) and its Q-factor versus the depth of blind hole H_1 with radius $R_1 = 1.5$ mm. (b) Resonant frequency of the TEM mode (f_2) and its Q-factor versus the length of the resonator H_2 with $py = 2.5$ mm, $pz = 2.3$ mm and a different radius R_2.

quarter-wavelength in the dielectric due to the loading effect of the quasi-TEM mode resonator.

The basic structure of the proposed dual-mode MDR is formed preliminary by two perpendicularly inserted metalized cylindrical posts. As shown in Fig. 3, because the aspect ratios of the lateral and longitudinal dimensions of the two resonators in the shared dielectric cavity are very different, the mode field patterns are dissimilar and so are the unloaded Q-factors. Since both modes are fundamental modes, their occupied common volume is minimum, spurious-free frequency bands are widest, and the dual-mode volume saving ratio is the highest.

B. Control of Dual-Mode Coupling

Different from conventional dual-mode resonators in which two degenerate modes are employed, the field distributions of the two dissimilar modes in the proposed dual-mode resonator are not strictly orthogonal to each other. Therefore, certain coupling between the two modes is inevitable, especially when the two orthogonal posts are placed electrically close to each other.

Besides adjusting the relative positions of the two cylindrical posts to control the intermode coupling to a limited extent, an additional partial-height metalized post between the two resonators can be introduced to further control (mainly reduce) the coupling between the two dissimilar modes. As shown in Fig. 1(c), the coupling control post is inserted into the resonator cavity between the two cylindrical posts along the

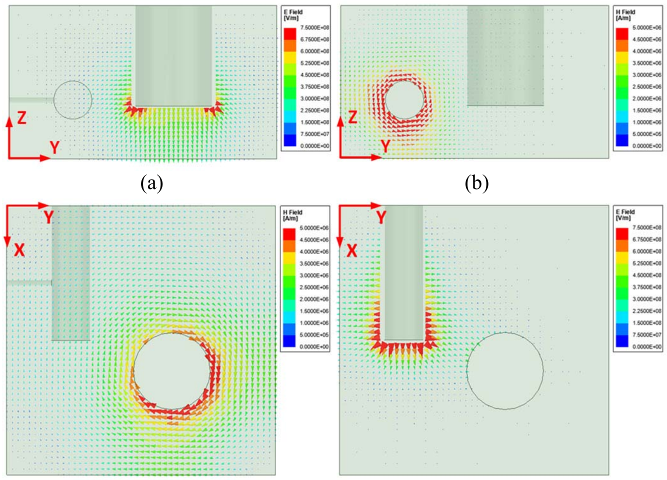

(a) (b) (c) (d)

Fig. 3. Electric and magnetic field patterns of the two fundamental modes in the dual-mode MDR at 2.6 GHz. (a) E-field of the quasi-TEM mode (mode 1). (b) H-field of the TEM mode (mode 2). (c) H-field of the quasi-TEM mode (mode 1). (d) E-field of the TEM mode (mode 2). When plotting the fields of one mode, the other mode is deliberately detuned.

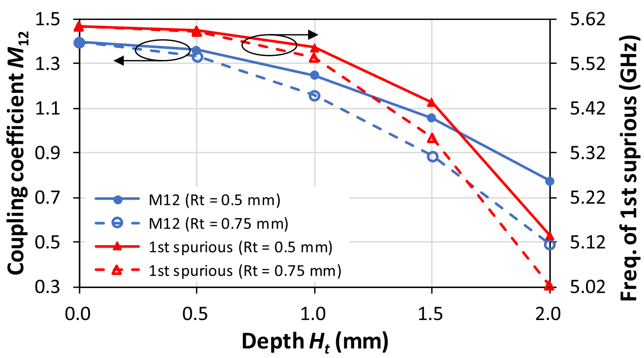

Fig. 4. Coupling coefficient M_{12} and the frequency of the first spurious mode versus the depth of decoupling post H_t with tx = 3.7 mm and ty = 3.6 mm.

vertical direction from the bottom surface of the cavity. The coupling control post from the bottom can effectively reduce the magnetic coupling between the two modes mainly by increasing the electric field coupling and, thus, can be named a "decoupling post." Oppositely, when a coupling control post is inserted vertically from the top surface of the cavity, the intermode coupling is increased. Nevertheless, in most cases, one only needs to reduce the coupling instead of increasing the coupling.

Fig. 4 shows the variation of the coupling coefficient of the two dissimilar modes in the dual-mode resonator versus the depth H_t of the "decoupling post" with a different radius R_t. The horizontal position of the post in this parametric study is set to tx = 3.7 mm and ty = 3.6 mm. The position of the horizontal post is the same as that of the previous analysis, and the offset distance d is set to 1.2 mm herein. The coupling coefficient M_{12} of the two approximately and synchronously tuned resonators of dissimilar modes can be calculated by the

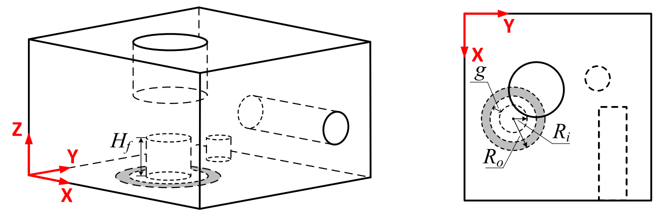

(a) (b)

Fig. 5. Schematic of coaxial feeding structure with an annular insulative gap around feeding probe. (a) Isometric view. (b) Top view.

following simplified formula [31]:

$$M_{12} = \frac{f_{p1}^2 - f_{p2}^2}{f_{p1}^2 + f_{p2}^2} \cdot \frac{f_0}{\mathrm{BW}} \tag{1}$$

where f_{p1} and f_{p2} are the resonant frequencies of the two coupled modes, and the center frequency f_0 and the bandwidth (BW) are set to 2.6 GHz and 160 MHz, respectively. It can be seen that the deeper the "decoupling post" is inserted from the bottom surface, the smaller the coupling becomes, and the larger the radius R_t is the less the coupling becomes. Fig. 4 also shows the trend of the first spurious mode in the resonator, indicating that the longer and thicker the decoupling post is, the closer to the passband the first spurious mode turns out to be. Therefore, there exists a tradeoff between the coupling control and the spurious performance. A compromised solution is that more than one decoupling post can be used.

It is worth mentioning that introducing the coupling control post will not affect the Q-factors of the two resonant modes noticeably. In addition, a design-in coupling control post provides much convenience in post-fabrication fine-tuning by slightly scratching the inner coating surface of the coupling control post.

III. Possible Coupling Configurations

In order to realize different filter characteristics by employing the proposed dual-mode resonator, the I/O coupling, intercavity coupling, and possible coupling configurations for higher-order filter applications should be addressed in a realizable manner and will be discussed in detail in this section.

A. I/O Coupling

As shown in Fig. 5, the I/O coupling structure includes a coaxial feeding probe with height H_f and radius R_i extending from the bottom of the dielectric block close to the vertical blind hole; thus, the quasi-TEM mode can be excited by the vertical field component of the fringe field of the feeding probe. The radius of the outer conductor is R_o that determines the port impedance. To prevent the input/output feeding probe from being short-circuited with the metalized outer surface of the dielectric block, an annular insulative gap is trimmed between the outer conductive layer and the feeding probe, thus forming a shunt capacitor to the ground. The size of the solder pad of the probe is controlled by dimension g, and the I/O coupling can be easily controlled by adjusting height H_f, radius R_i, and width g.

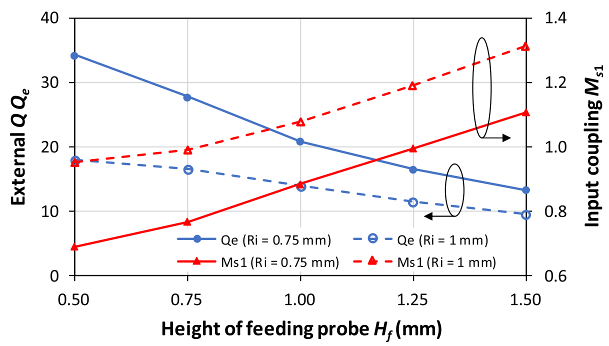

Fig. 6. External Q and input coupling coefficient M_{s1} versus the height of feeding probe H_f with fixed width $g = 0.5$ mm and a different radius R_i.

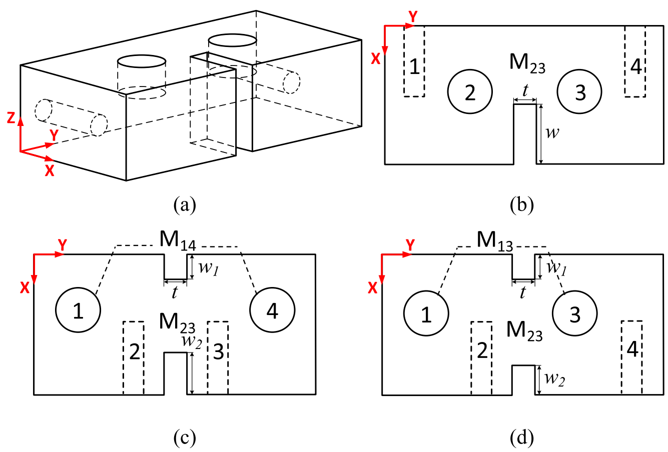

Fig. 7. Possible intercavity coupling structures between two proposed dual-mode resonators for fourth-order modules. (a) and (b) Isometric view and top views of the arrangement coupled by two quasi-TEM modes. (c) Top view of the arrangement coupled by two TEM modes. (d) Top view of the arrangement coupled by two dissimilar TEM modes.

Fig. 6 shows the parametric study of the external Q and input coupling coefficient M_{s1} versus the height of feeding probe H_f with $g = 0.5$ mm and a different radius R_i. The feeding probe is placed right below the vertical blind hole, and the outer conductor radius R_o is set to 2.3 × R_i to ensure a 50-Ω port impedance of an air-filled coaxial connector. The center frequency f_0 and BW for calculating input coupling M_{s1} are set to 2.6 GHz and 160 MHz, respectively. It can be found that the external Q decreases with the increase of H_f and R_i, and a wide range of coupling values can be reached. In practice, the desired input coupling coefficient is realized mainly by adjusting H_f and R_i, while g can be adjusted in the fine-tuning process. Apparently, the I/O structure is compatible with surface-mount process on a printed circuit board (PCB).

B. Intercavity Coupling

To combine two or more proposed dual-mode resonators, three basic intercavity coupling arrangements can be made between either the same or different types of resonant modes. For example, Fig. 7(a) and (b) shows one possible coupling configuration for a fourth-order filter consisting of two proposed dual-mode resonators coupled between two quasi-TEM modes. The intercavity coupling M_{23} can be controlled by adjusting the width w and the thickness t of the partial-width coupling window.

In Fig. 7(c), two TEM modes supported by two horizontal blind holes in two dual-mode resonators are coupled. Similarly, the coupling between two TEM modes can be controlled by adjusting the width w_2 of the coupling window between two horizontal blind holes. In this configuration, a parasitic cross-coupling M_{14} between two nonadjacent quasi-TEM modes (resonators 1 and 4) may exist since the magnetic field of the quasi-TEM mode dominates the whole cavity, forming a cascaded quartet (CQ) section that will create a pair of complex TZs. The cross-coupling M_{14} can be adjusted by the width w_1 of the coupling window. Fig. 7(d) shows an asymmetric configuration in which the two dual-mode resonators are cascaded by coupling two dissimilar modes. Besides controlling the width w_2 of the partial-width window, an aforementioned "coupling control post" can be added to control the intercavity coupling M_{23} if needed. Note that a parasitic cross-coupling M_{13} may exist between two quasi-TEM modes (resonators 1 and 3), forming a cascaded trisection (CT) unit, which will create an imaginary TZ at the upper side of the filter passband. Similarly, the cross-coupling M_{13} can be adjusted by tuning the width w_1.

Having introduced the three basic intercavity coupling configurations, various filter topologies with arbitrary order can be realized by simply cascading the modules in Fig. 7 or coupling one or more single-mode resonators between two dual-mode resonators, showing great flexibility in the realization of compact monoblock dielectric filters.

IV. Two Design Examples

After introducing the basic characteristics of the proposed dual-mode MDR and its possible intercavity coupling configurations, the way of designing a bandpass filter using such a dual-mode resonator becomes very straightforward. First, a coupling matrix with achievable coupling topology to satisfy the prescribed filter characteristic should be synthesized with a standard procedure [32]. Then, within the given size restriction, the dimension of each dual-mode resonator can be determined, and the relative position of two blind holes needs to be appropriately arranged by trading off the desired coupling coefficient and unloaded Q-factors. The initial dimension design of the resonators and the coupling structures can be done with the help of the full-wave EM software ANSYS HFSS. The final EM design of a filter and the tuning of its fabricated prototype rely on the computer-aided tuning technique described in [33]–[35].

In this section, two design examples including one EM-designed six-pole bandpass filter and one fabricated ten-pole bandpass filter targeting 5G wireless system base station applications are presented, illustrating the design process and demonstrating the features of the proposed dual-mode MDR.

A. Six-Pole Inline Bandpass Filter

In this example, a six-pole inline bandpass filter with center frequency $f_0 = 3.5$ GHz and BW = 200 MHz is synthesized

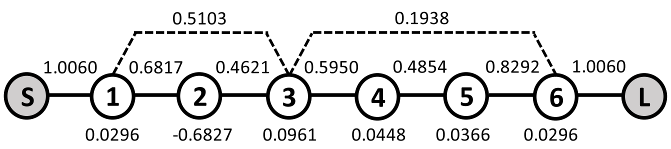

Fig. 8. Coupling topology with synthesized coupling coefficients of the EM designed six-pole inline bandpass filter.

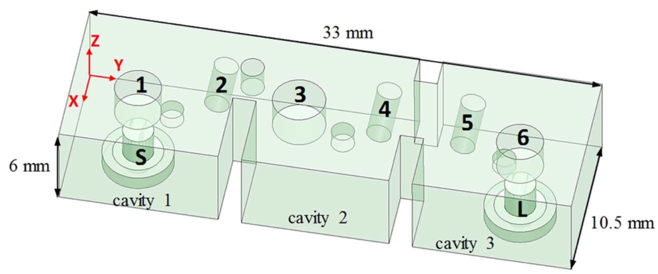

Fig. 9. EM model (perspective view) of the six-pole filter with its outer dimensions and serial numbers of resonators.

and EM designed. The return loss level is 20 dB, and a pure imaginary TZ at normalized low-pass frequency $\Omega = 1.3$ rad/s is prescribed to ensure a rejection level of 28 dB on the right-hand side of the passband. Moreover, a pair of complex TZs at $-0.04 \pm j1$ rad/s give a group delay equalization over approximately 60% of the passband. The coupling topology with the synthesized coupling coefficients is superposed in Fig. 8, where the trisection with cross-coupling M_{13} creates the TZ and the quartet with cross-coupling M_{36} realizes a self-equalized complex TZ pair.

As to the physical realization of the filter, three dual-mode MDRs with relative permittivity $\varepsilon_r = 20.6$ are used, and the size of each cavity is $10.5 \times 11 \times 6$ mm^3, with the total size of the cascaded six-pole inline filter of $33 \times 10.5 \times 6$ mm^3, which means a 50% volume reduction compared to a conventional single-mode monoblock dielectric filter.

The arrangement for the three dual-mode resonators is shown in Fig. 9, where cavity 2 and cavity 3 are coupled between two TEM modes in the way shown in Fig. 7(c), whereas cavity 1 and cavity 2 are coupled between two dissimilar modes in the way shown in Fig. 7(d). As discussed in Sections II and III, all coupling elements can be adjusted independently in the EM design process: the resonant frequency of each resonator can be adjusted by changing the depth of the vertical blind hole or the length of the horizontal blind hole, the interresonator coupling in each dual-mode cavity can be adjusted by the relative position of the resonator pair and the preset "decoupling post" between them, the intercavity coupling and the cross-coupling can be adjusted by the width of the coupling window, and a "coupling post" is additionally formed between cavity 1 and cavity 2 to increase the coupling M_{23}.

The dimensional parameters of the resonators and coupling structures are labeled in the top and the side views of the EM model in Fig. 10, and the values of those parameters after the fine-tuning process are listed in Table I. The EM simulation results with lossless materials are shown in Fig. 11(a) and (b),

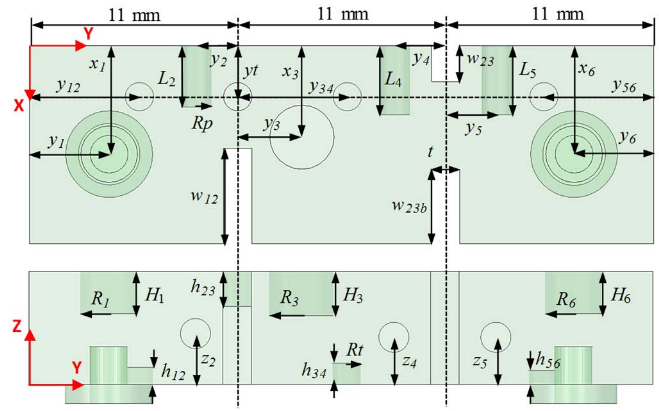

Fig. 10. EM model (top and side view) of the six-pole filter with its dimensional parameters.

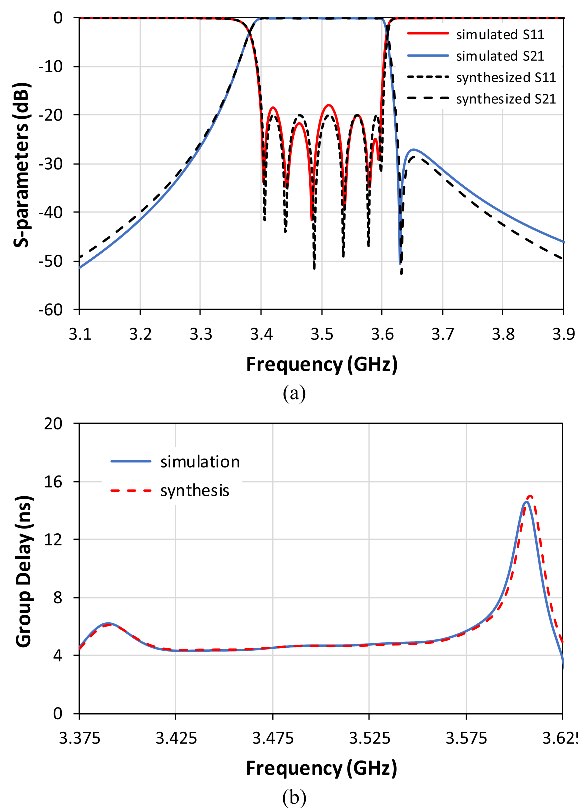

Fig. 11. EM simulated and ideal synthesized responses of the EM designed six-pole filter. (a) Magnitude of S-parameters. (b) In-band group delay response.

where solid lines are the simulated data of the EM model and dashed lines are the ideal synthesized responses given by the coupling diagram in Fig. 8 for comparison. It can be observed that the EM simulated responses show good agreement with the ideal synthesized responses, which validates the proposed dual-mode MDR filter from a theoretical perspective.

B. Ten-Pole Symmetric Bandpass Filter

In this example, a ten-pole symmetric bandpass filter prototype with a target passband of 2515–2680 MHz, which is

TABLE I
DIMENSIONS OF THE EM MODEL IN FIG. 10 (UNIT: mm)

x_1	y_1	R_1	H_1	y_2	z_2	L_2	Rp	Rt	y_{12}	h_{12}	t
5.75	4.2	1.5	2.26	2.2	2.7	3.26	0.8	0.75	5.8	0.9	1.5
x_3	y_3	R_3	H_3	y_4	z_4	L_4	yt	h_{23}	y_{34}	h_{34}	w_{12}
4.85	3.4	1.75	2.37	2.7	2.5	3.66	2.7	1.86	5.8	1.12	5.05
x_6	y_6	R_6	H_6	y_5	z_5	L_5	w_{23}	w_{23b}	y_{56}	h_{56}	
5.75	4.2	1.5	2.26	2.7	2.5	3.66	1.9	3.9	5.8	0.75	

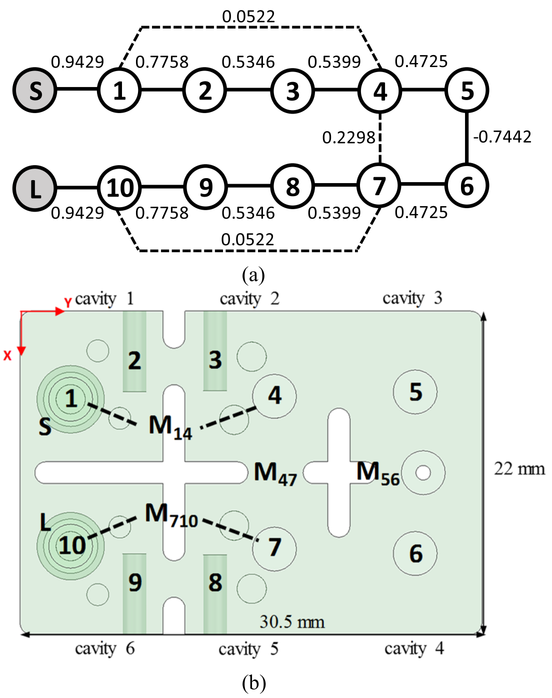

Fig. 12. (a) Coupling topology with synthesized coupling coefficients of the ten-pole symmetric bandpass filter (all self-coupling coefficients are zero and are omitted herein). (b) Physical layout (top view) of the filter with serial numbers of resonators, negative coupling, and cross-couplings.

a 2.6-GHz 5G new radio (NR) frequency band, is designed and experimentally verified. The designated return loss level is set at 18 dB, and a pair of pure imaginary TZs at normalized low-pass frequency $\Omega = \pm 1.13$ rad/s are prescribed to provide a rejection level of 35 dB on both sides of the passband. A filter circuit model with the Chebyshev response that satisfies the specifications is synthesized, and the coupling topology with coupling coefficients is given in Fig. 12(a), where the quartet with cross-coupling M_{47} creates the pair of symmetric pure imaginary TZs. Considering the parasitic couplings M_{14} and $M_{7,10}$ caused by two cascaded dual-mode resonators, two mirror-image TZ pairs at $\Omega = \pm j2$ rad/s are added in the initial synthesis process. Since the filter characteristic is symmetric, the self-coupling coefficients of each resonator are zero and are omitted in the coupling topology diagram.

Different from the previous example, the realization of this filter takes a double-folded structure with four side-by-side dual-mode resonators and two single-mode resonators. The dielectric material used for the prototype filter is $MgTiO_3$-$CaTiO_3$ (MCT) compounds ceramic. Although its

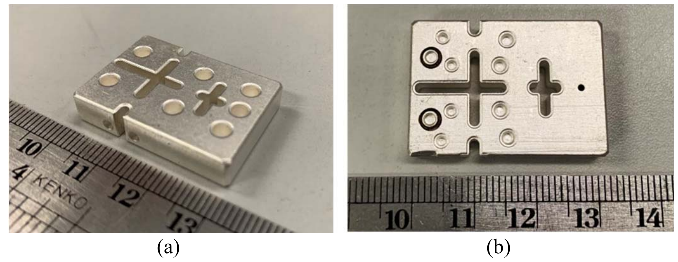

Fig. 13. Photographs of the fabricated ten-pole MDR filter. (a) Top and side views. (b) Bottom view of the filter with input/output ports and "decoupling posts" shown.

specified relative permittivity ε_r is 20.6 and the loss tangent $\tan\delta = 5 \times 10^{-5}$, due to manufacturing variation, the measured ε_r that is used in the design is 19.5. The size of each MDR cavity is $11 \times 10.5 \times 6$ mm^3 so that the total size of the ten-pole filter prototype is $30.5 \times 22 \times 6$ mm^3, which provides a 40% volume reduction compared to the conventional single-mode solution. The arrangement of the six resonator cavities is shown in Fig. 12(b), where cavities 1 and 2 and cavities 5 and 6 are coupled between two similar TEM modes in the way shown in Fig. 7(c). The quartet section is formed by the single-mode resonators 5 and 6 and the quasi-TEM resonators 4 and 7. Note that, different from the general quartet section, the polarities of couplings M_{56} and M_{47} are shifted herein, and the positive cross-coupling M_{47} is realized by a partial-width window between resonators 4 and 7, whereas the negative coupling M_{56} can be realized by a blind hole or a via hole with an insulator gap on one end, thus creating a strong capacitive coupling between resonators 5 and 6.

The designed ten-pole filter is fabricated and fine-tuned. The photographs of the filter prototype hardware are shown in Fig. 13, where the silver conductive layer is coated outside of the dielectric block. It can be seen in Fig. 13(b) that, for each dual-mode resonator cavity, two "decoupling posts" are introduced along the vertical direction from the bottom surface. Different from the tuning method of the conventional metal cavity coaxial resonator filter, in which tuning screws are preset on the metallic top lid for post-fabrication tuning, the monoblock dielectric filter can only be fine-tuned by irreversibly scratching the conductive surface at strategic spots to compensate for the fabrication error, presenting a limited tuning range.

The measured responses of the fabricated filter prototype after fine-tuning are shown in Fig. 14, where solid lines are the measured data and dashed lines are the responses of the synthesized circuit model shown in Fig. 12(a) for comparison. Considering the loss effect of the dielectric material and conductive layer of the filter hardware, estimated unloaded Q values are added to each resonator in the circuit model: $Q = 1000$ for quasi-TEM mode resonators (1, 4, 7, and 10), $Q = 700$ for TEM mode resonators (2, 3, 8, and 9), and $Q = 1100$ for single-mode resonators (5, 6). Note that the estimated Q values are slightly lower than those of previous parametric analysis due to the imperfection of the coating

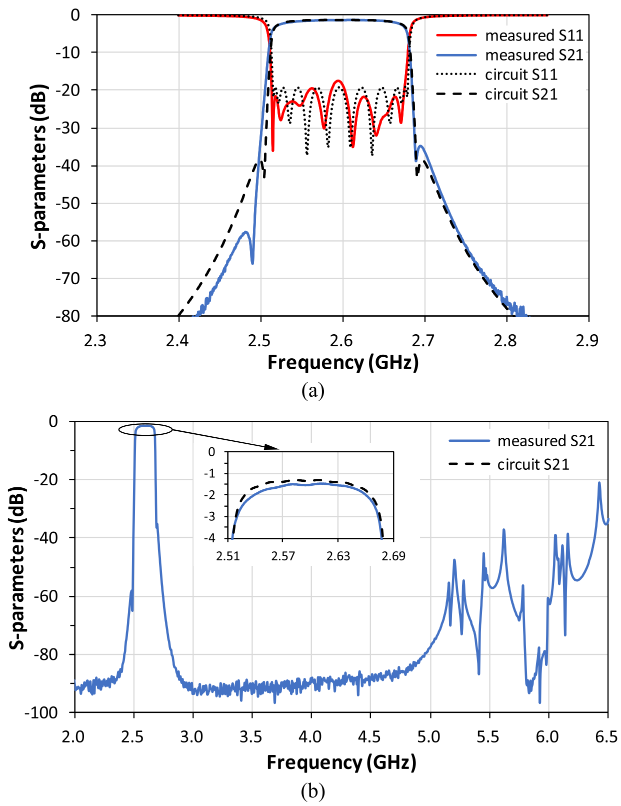

Fig. 14. Experimental and the synthesized circuit model results of the fabricated ten-pole MDR filter. (a) Measured S-parameters (solid lines) near the passband and circuit model responses (dashed lines) with estimated loss. (b) Measured $|S_{21}|$ response in a wideband and comparison of insertion loss with the circuit model response.

process and the smaller effective volume of a resonator. It can be seen from Fig. 14(a) that the filter realizes a return loss under 18 dB within the prescribed passband, and the measured insertion loss at f_0 is 1.55 dB. An asymmetry of sidelobes can be observed near the passband, which is caused by the dispersion effect of the negative coupling structure M_{56}. Moreover, due to the patching process of the conductive layer over the overscratched areas in fine-tuning, the measured insertion loss shown in Fig. 14(b) is found worse than that of the circuit model with estimated Q values but is still at an acceptable level. Fig. 14(b) also shows a wideband response of the filter. Although some spurious resonances attributed by those "decoupling posts" exist between 5 and 6 GHz, a wide spurious-free frequency band (below -40 dB) up to 5.5 GHz (more than $2.1 \times f_0$) can be obtained, justifying a superior spurious performance of such a dual-mode MDR filter.

V. Conclusion

In this work, a novel dual-mode resonator for compact MDR bandpass filters is proposed. Different from previous degenerate dual-mode DRs, the proposed dual-mode resonator adopts two dissimilar TEM modes by forming two perpendicular metalized blind holes in a silver-coated cuboid-shaped dielectric block. Compared to the existing single-mode solution, the proposed dual-mode resonator can provide a maximum space-saving ratio with acceptable sacrifice in unloaded Q while maintaining a wide spurious-free rejection band at the same time. The basic structure and characteristics of the dual-mode resonator are presented in detail. Importantly, the inevitable coupling between the two dissimilar modes in one cavity can be effectively controlled by introducing one or more "coupling/decoupling metal posts." Moreover, the method for I/O coupling and possible coupling configurations between resonators are also presented. A six-pole inline bandpass filter is EM designed, and a ten-pole monoblock dielectric filter using mixed dual- and single-mode resonators is designed, fabricated, and measured. Good agreement between the theoretical and experimental results justifies the proposed dual-mode resonator and demonstrates the claimed features. It can be expected that the MDR filters with the proposed dual-mode MDR can be a viable option for the M-MIMO radio units in 5G and future wireless communication systems, in which the filter size matters.

Acknowledgment

The authors would like to thank Z. Duan of GrenTech RF (Shenzhen) for fabricating the hardware in this article and helpful suggestions in designing the prototype filters.

References

[1] W. H. Harrison, "A miniature high-Q bandpass filter employing dielectric resonators," *IEEE Trans. Microw. Theory Techn.*, vol. MTT-16, no. 4, pp. 210–218, Apr. 1968.

[2] S. B. Cohn, "Microwave bandpass filters containing high-Q dielectric resonators," *IEEE Trans. Microw. Theory Techn.*, vol. MTT-16, no. 4, pp. 218–227, Apr. 1968.

[3] J. K. Plourde and C.-L. Ren, "Application of dielectric resonators in microwave components," *IEEE Trans. Microw. Theory Techn.*, vol. MTT-29, no. 8, pp. 754–770, Aug. 1981.

[4] S. J. Fiedziuszko, "Dual-mode dielectric resonator loaded cavity filters," *IEEE Trans. Microw. Theory Techn.*, vol. MTT-30, no. 9, pp. 1311–1316, Sep. 1982.

[5] I. C. Hunter, J. D. Rhodes, and V. Dassonville, "Dual-mode filters with conductor-loaded dielectric resonators," *IEEE Trans. Microw. Theory Techn.*, vol. 47, no. 12, pp. 2304–2311, Dec. 1999.

[6] L. Accatino, G. Bertin, M. Mongiardo, and G. Resnati, "Dual-mode filters with grooved/splitted dielectric resonators for cellular-radio base stations," *IEEE Trans. Microw. Theory Techn.*, vol. 50, no. 12, pp. 2882–2889, Dec. 2002.

[7] L. Pelliccia, F. Cacciamani, C. Tomassoni, and R. Sorrentino, "Ultra-compact filters using TM dual-mode dielectric-loaded cavities with asymmetric transmission zeros," in *IEEE MTT-S Int. Microw. Symp. Dig.*, Jun. 2012, pp. 1–3.

[8] H. Hu and K.-L. Wu, "A TM11 dual-mode dielectric resonator filter with planar coupling configuration," *IEEE Trans. Microw. Theory Techn.*, vol. 61, no. 1, pp. 131–138, Jan. 2013.

[9] V. Walker and I. C. Hunter, "Design of triple mode TE_{01}spl delta// resonator transmission filters," *IEEE Microw. Wireless Compon. Lett.*, vol. 12, no. 6, pp. 215–217, Jun. 2002.

[10] J. Hattori, T. Wada, H. Kubo, and Y. Ishikawa, "2 GHz band quadruple mode dielectric resonator filter for cellular base station," in *IEEE MTT-S Int. Microw. Symp. Dig.*, Jun. 2003, pp. 933–936.

[11] M. Memarian and R. R. Mansour, "Quad-mode and dual-mode dielectric resonator filters," *IEEE Trans. Microw. Theory Techn.*, vol. 57, no. 12, pp. 3418–3426, Dec. 2009.

[12] C. Tomassoni, S. Bastioli, and R. V. Snyder, "Compact mixed-mode filter based on TE_{101} cavity mode and TE_{01} dielectric mode," *IEEE Trans. Microw. Theory Techn.*, vol. 64, no. 12, pp. 4434–4443, Dec. 2016.

[13] R. L. Sokola and C. Choi, "Ceramic bandpass filter," U.S. Patent 4 431 977, Feb. 14, 1984.

[14] D. M. DeMuro and D. Agahi-Kesheh, "Monolithic ceramic filter with bandstop function," U.S. Patent 4 823 098, Apr. 18, 1989.

[15] H.-W. Yao, C. Wang, and A. K. Zaki, “Quarter wavelength ceramic combline filters,” *IEEE Trans. Microw. Theory Techn.*, vol. 44, no. 12, pp. 2673–2679, Dec. 1996.

[16] Y. Konishi, “Novel dielectric waveguide components-microwave applications of new ceramic materials,” *Proc. IEEE*, vol. 79, no. 6, pp. 726–740, Jun. 1991.

[17] K. Sano and M. Miyashita, “Dielectric waveguide filter with low profile and low-insertion loss,” *IEEE Trans. Microw. Theory Techn.*, vol. 47, no. 12, pp. 2299–2303, Dec. 1999.

[18] I. C. Hunter and M. Y. Sandhu, “Monolithic integrated ceramic waveguide filters,” in *IEEE MTT-S Int. Microw. Symp. Dig.*, Jun. 2014, pp. 1–3.

[19] X. Wang, K.-L. Wu, and W.-Y. Yin, “A novel surface-mounted monoblock dielectric filter,” *IEEE Trans. Compon., Packag., Manuf. Technol.*, vol. 4, no. 11, pp. 1822–1827, Nov. 2014.

[20] X. Wang and K.-L. Wu, “A TM_{01} mode monoblock dielectric filter,” *IEEE Trans. Microw. Theory Techn.*, vol. 62, no. 2, pp. 275–281, Feb. 2014.

[21] Y. Rong, K. A. Zaki, M. Hageman, D. Stevens, and J. Gipprich, “Low-temperature cofired ceramic (LTCC) ridge waveguide bandpass chip filters,” *IEEE Trans. Microw. Theory Techn.*, vol. 47, no. 12, pp. 2317–2324, Dec. 1999.

[22] L. Qiu, X. Zhang, Z. Liu, and Z. Shen, “Dielectric resonator and filter,” W.O. Patent 2017/088195 A1, Jun. 1, 2017.

[23] B. Yuan, “Filter and transceiver comprising dielectric body resonators having frequency adjusting holes and negative coupling holes,” U.S. Patent 9 998 163 B2, Jun. 12, 2018.

[24] U. Rosenberg and S. Amari, “A novel band-reject element for pseudoelliptic bandstop filters,” *IEEE Trans. Microw. Theory Techn.*, vol. 55, no. 4, pp. 742–746, Apr. 2007.

[25] M. Politi and A. Fossati, “Direct coupled waveguide filters with generalized Chebyshev response by resonating coupling structures,” in *Proc. 40th Eur. Microw. Conf.*, 2010, pp. 966–969.

[26] H. Kojima, M. Nakahori, K. Matsutani, K. Kuroda, and K. Onaka, “A compact 28 GHz bandpass filter using quartz folded waveguide,” in *IEEE MTT-S Int. Microw. Symp. Dig.*, Jun. 2018, pp. 1110–1113.

[27] K. Matsutani *et al.*, “Miniaturized quartz waveguide filter using double-folded structure,” in *IEEE MTT-S Int. Microw. Symp. Dig.*, Jun. 2019, pp. 1201–1204.

[28] D. R. Hendry and A. M. Abbosh, “Triple-mode ceramic cavity filters with wide spurious-free performance,” *IEEE Trans. Microw. Theory Techn.*, vol. 65, no. 10, pp. 3780–3788, Oct. 2017.

[29] A. A. S. Blas, J. C. Melgarejo, V. E. Boria, and M. Guglielmi, “Novel solution for the coaxial excitation of inductive rectangular waveguide filters,” in *Proc. 48th Eur. Microw. Conf. (EuMC)*, Sep. 2018, pp. 89–92.

[30] A. A. San-Blas, M. Guglielmi, J. C. Melgarejo, A. Coves, and V. E. Boria, “Design procedure for bandpass filters based on integrated coaxial and rectangular waveguide resonators,” *IEEE Trans. Microw. Theory Techn.*, vol. 68, no. 10, pp. 4390–4404, Oct. 2020.

[31] J.-S Hong and M. J. Lancaster, *Microstrip Filters for RF/Microwave Applications*. New York, NY, USA: Wiley, 2001, pp. 251–255.

[32] R. J. Cameron, C. M. Kudsia, and R. R. Mansour, *Microwave Filters for Communication Systems*. Hoboken, NJ, USA: Wiley, 2007.

[33] M. Meng and K.-L. Wu, “An analytical approach to computer-aided diagnosis and tuning of lossy microwave coupled resonator filters,” *IEEE Trans. Microw. Theory Techn.*, vol. 57, no. 12, pp. 3188–3195, Dec. 2009.

[34] H. Hu and K.-L. Wu, “A generalized coupling matrix extraction technique for bandpass filters with uneven-Qs,” *IEEE Trans. Microw. Theory Techn.*, vol. 62, no. 2, pp. 244–251, Feb. 2014.

[35] P. Zhao and K.-L. Wu, “Model-based vector-fitting method for circuit model extraction of coupled-resonator diplexers,” *IEEE Trans. Microw. Theory Techn.*, vol. 64, no. 6, pp. 1787–1797, Jun. 2016.

Yuliang Chen (Graduate Student Member, IEEE) received the B.Eng. degree in electromagnetic field and wireless technology from Northwestern Polytechnical University, Xi’an, China, in 2017. He is currently pursuing the Ph.D. degree at the Department of Electronic Engineering, The Chinese University of Hong Kong, Hong Kong SAR.

His current research interests include miniaturization techniques and robot automatic tuning of microwave filters for wireless communication.

Yan Zhang received the B.S. degree in electronic engineering from the University of Electronic Science and Technology of China, Chengdu, China, in 2017. She is currently pursuing the Ph.D. degree at The Chinese University of Hong Kong, Hong Kong.

Her current research interests include synthesis and tuning of filters with dispersive couplings and irregular topologies.

Ms. Zhang was a recipient of Hong Kong Ph.D. Fellowship.

Ke-Li Wu (Fellow, IEEE) received the B.S. and M.Eng. degrees from the Nanjing University of Science and Technology, Nanjing, China, in 1982 and 1985, respectively, and the Ph.D. degree from Laval University, Quebec, QC, Canada, in 1989.

From 1989 to 1993, he was a Research Engineer with McMaster University, Hamilton, ON, Canada. He joined COM DEV (now Honeywell Aerospace), Cambridge, ON, Canada, in 1993, where he was a Principal Member of Technical Staff. Since 1999, he has been with The Chinese University of Hong Kong, Hong Kong, where he is currently a Professor and the Director of the Radio Frequency Radiation Research Laboratory. His current research interests include electromagnetic (EM)-based circuit domain modeling of high-speed interconnections, robot automatic tuning of microwave filters, decoupling techniques of multi-input and multi-output (MIMO) antennas, and Internet of Things (IoT) technologies.

Dr. Wu is a member of the IEEE MTT-5 Technical Committee. He was a recipient of the 1998 COM DEV Achievement Award and the Asia-Pacific Microwave Conference Prize twice in 2008 and 2012, respectively. He was an Associate Editor of the IEEE TRANSACTIONS ON MICROWAVE THEORY AND TECHNIQUES from 2006 to 2009.